Journal of Materials Chemistry B

Accepted Manuscript

ROYAL SOCIETY OF CHEMISTRY

www.rsc.org/materialsB

Sub-10 nm $BaLaF_5$:Mn/Yb/Er nanoprobes for dual-modal synergistic *in vivo* upconversion luminescent and X-ray bioimaging

Ling Rao,[a,b] Wei Lu,[c] Tianmei Zeng,[a] Zhigao Yi, [a,b] Haibo Wang, [a,b] Hongrong Liu[a] and Songjun Zeng[*a]

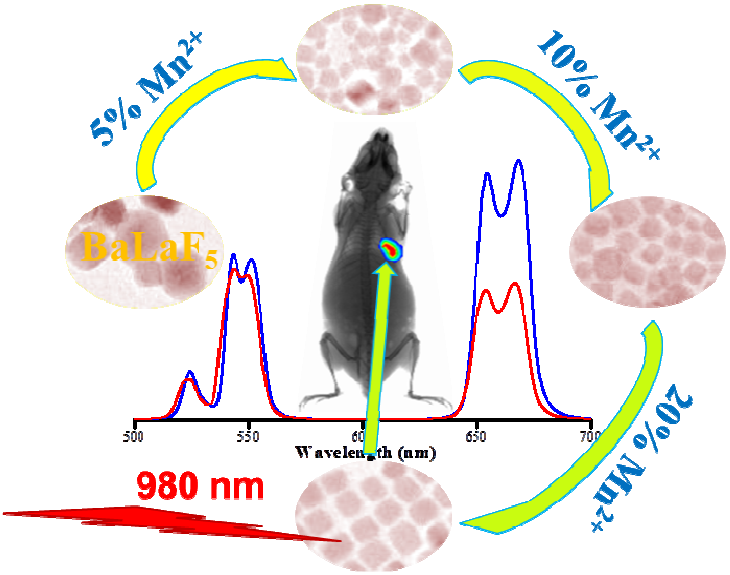

Sub-10 nm ultra-small $BaLaF_5$:Mn/Yb/Er nanoparticles were synthesized by a simple solvothermal method for *in vivo* upconversion luminescence and X-ray bioimaging.

Cite this: DOI: 10.1039/c0xx00000x

www.rsc.org/xxxxxx

ARTICLE TYPE

Sub-10 nm $BaLaF_5$:Mn/Yb/Er nanoprobes for dual-modal synergistic *in vivo* upconversion luminescent and X-ray bioimaging

Ling Rao,[a,b,d] Wei Lu,[c,d] Tianmei Zeng,[a] Zhigao Yi, [a,b] Haibo Wang, [a,b] Hongrong Liu[a] and Songjun Zeng[*a]

Received (in XXX, XXX) Xth XXXXXXXXX 20XX, Accepted Xth XXXXXXXXX 20XX

DOI: 10.1039/b000000x

Samll-sized $BaLaF_5$:Mn/Yb/Er upconversion nanoparticles (UCNPs) were successfully synthesized for dual-modal X-ray and upconversion (UC) luminescent bioimaging by a simple solvothermal method. The size, shape, and UC luminescent intensity of the as-prepared UCNPs can be readily modified by changing the contents of Mn^{2+}. The size of the $BaLaF_5$ UCNPs doped with Mn^{2+} decreased largely compared with the Mn-free UCNPs. When increasing the content of Mn^{2+} from 5%-20%, the size of UCNPs was gradually increased from 6.5 nm to 9.7 nm. The as-prepared $BaLaF_5$ UCNPs doped with 20% Mn^{2+} present intense UC luminescence. The *in vitro* UC luminescence imaging of HeLa cells and localized spectra detected from HeLa cells and background based on these $BaLaF_5$:Mn/Yb/Er (20/20/2%) UCNPs indicate this sample can serve as ideal bioprobes with absence of autofluorescence under the excitation of 980 nm laser. Moreover, an obvious UC signal was observed in *in vivo* UC bioimaging, demonstrating these $BaLaF_5$:Mn/Yb/Er (20/20/2%) UCNPs can also be used as bioprobes for whole body optical bioimaging. In addition, owing to the high X-ray mass absorption coefficients of Ba^{2+}, La^{3+} and the doped Yb^{3+}, the simultaneous X-ray and UC *in vivo* bioimaging of a nude mouse further demonstrate the as-prepared UCNPs can be successfully used as dual-modal bioprobes. *Ex vivo* UC bioimaging revealed these UCNPs gathered at the lung of a mouse at initial time, demonstrating this sample was suitable for detection of the lung diseases. In addition, the cytotoxicity test showed the UCNPs possessed little toxicity. Therefore, the small-sized $BaLaF_5$:Yb/Er/Mn UCNPs are ideal nanoprobes for dual-modal UC luminescent/X-ray bioimaging with non-autofluorescence, and enhanced detection of the lung diseases.

1. Introduction

Lanthanide doped UCNPs have evoked considerable interest as a new generation of fluorescent probes for bioimaging because of their unique UC property of converting low energy irradiation to high energy emissions via a two-photon or multi-photon process. [1-18] This unique optical property is crucial for the applications of these lanthanide doped UC nano-materials in bioimaging. During the past decades, various fluorescent probes such as organic dyes, fluorescent proteins, and quantum dots have been developed and widely used in bioimaging field.[19-21] Compared with the conventional developed optical bioimaging probes, the UC luminescent materials possess some intrinsic advantages: low toxicity, deep penetration, reduced autofluorescence, excellent photostability, et al. [22-31] These features make them highly suitable for X-ray and UC bioimaging *in vivo*, which require bright luminescence, extremely small size, and weak autofluorescence. [32-39]

It is well known that small nanoparticles are easily expelled from *in vivo,* and more suitable for application in biomedical applications, such as drug delivery, photodynamic therapy, various luminescent bioassays, owing to the low toxicity and little damage to the living body. [40-44] However, it is still a great challenge to synthesize intense UC luminescence of nanocrystals with small size, especially the diameter less than 10 nm.[41,45] Therefore, several efforts have been dedicated to achieving sub-10 nm nanoparticles with intense UC luminescence.[46] Recently, Liu's group synthesized sub-10 nm core-shell nanoparticles for dual-modal imaging and photothermal therapy via a thermal decomposition method.[47] Venkataramanan Mahalingam and his co-workers synthesized sub-5 nm Ln^{3+}-doped $BaLuF_5$ nanocrystals via thermal decomposition.[48] Li's group[41] reported sub-10 nm $NaLuF_4$ nanoparticles for in vivo bioimaging by a thermal decomposition method using Gd^{3+} doping. However, the thermal decomposition method needs stringent experimental conditions such as high temperature, inert gas protection, making the experimental process complex and laborious. Therefore, it is of significant importance to develop a simple method to achieve high quality sub-10 nm nanocrystals with controlled structure. On the other hand, fluoride was an excellent host material for its low phonon energy which minimize nonradiative losses and enable intense infrared-to-visible up-converting emissions. [49] As one of the important fluoride hosts, $BaLnF_5$ can not only possess excellent UC emission properties, but also have intrinsic different X-ray absorption coefficient of Ba and Ln, making these Ba-based hosts are ideal dual-modal probes for optical and X-ray bioimaging. [50-58] However, the nanoprobes based on the sub-10 nm ultra-small $BaLnF_5$ UCNPs for dual-modal bioimaging has

not been developed. Furthermore, shape, size and red UC fluorescence can be tuned by controlling the content of Mn^{2+} in the $NaLnF_4$ (Ln=Lu, Y) host materials.[59,60] But there was no any report about the tunable morphology and size of $BaLnF_5$ host by doping Mn^{2+}.

Therefore, we report a simple method to achieve small-sized nm ultra-small Ln^{3+}-doped $BaLaF_5$ UCNPs with tunable shape, size and UC emission by adjusting Mn^{2+} contents. These small-sized $BaLaF_5$ UCNPs are successfully applied in *in vitro* and *in vivo* UC luminescent bioimaging with absence of autofluorescence. Moreover, the synergistic dual-modal *in vivo* UC and X-ray imaging was demonstrated for the first time. And the biodistribution of these UCNPs was studied by *ex-vivo* UC luminescent bioimaging after 0.5 h systemic delivery of UCNPs.

2. Materials and methods

2.1 Chemicals and materials

Rare earth oxides were of 99.99% purity, which were dissolved in nitric acid at high temperature, and the concentrations of $La(NO_3)_3$, $Yb(NO_3)_3$ and $Er(NO_3)_3$ are 0.5 M, 0.5 M and 0.05 M, respectively. $BaCl_2$ (99.99%), $MnCl_2{\cdot}4H_2O$ and NH_4F were purchased from Sinopharm Chemical Reagent Co., China. Other chemicals (sodium hydroxide, oleic acid, ethyl alcohol) were used without any further purification.

2.2 One-pot solvothermal synthesis of small-sized $BaLaF_5$:Mn/Yb/Er UCNPs

Sub-10 nm $BaLaF_5$:20%Yb/2%Er UCNPs was synthesized by a solvothermal method with doping different Mn^{2+}.[61-63] 10 mL of ethanol and 20 mL of oleic acid were added into 2 mL deionized water containing 0.6 g NaOH under vigorously stirring. And then, 1 mL $BaCl_2$ (1 M) solution was added into the above mixture solution. After that, 1 mmol of $La(NO_3)_3$ (0.5 M), $Yb(NO_3)_3$ (0.5 M), $Er(NO_3)_3$ (0.05 M) and $MnCl_2$ (1 M) with the designed molar ratio of 78-x:20:2:x (x=0, 5, 10 and 20) was added into the mixture solution and the solvent was further stirred to become homogeneous. Finally, 6 mL NH_4F (1 M) was added. The prepared solution was then transferred into a 50 mL stainless Teflon-lined autoclave, which reacted completely at 200 ℃ for 24 h. Then the product was naturally cooled down to room temperature. Ethanol and deionized water was used to wash the mixture for three to four times to remove oleic acid and other solvents. Finally, the as-prepared $BaLaF_5$ UCNPs were put in a vacuum drying oven and dried at 60 ℃ for 24 h.

To convert these hydrophobic UCNPs to hydrophilic, a half of the $BaLaF_5$:20%Mn/20%Yb/2%Er was dispersed in 2.64 mL chloroform and 0.79 g sodium dodecylsulphate (SDS) was added. The chloroform was evaporated after the mixture was vigorously stirred for 5 h at the room temperature. [48]

2.3 Characterization

The crystal phase of the as-prepared $BaLaF_5$:Mn/Yb/Er UCNPs were characterized by a Rigaku D/max 2500 System X-ray diffractometer (XRD) with Cu-Kα (λ = 0.15406 nm) radiation in the 2θ range from 20° to 80°. The morphology of these nanocrystals was characterized by a transmission electron microscope (TEM, JEOL-2100F) at an acceleration voltage of 200 kV. At room temperature, the UC emission spectra were measured in conjunction with an excitation source of a 980 nm laser diode with an increasing pump power from 0.2 W to 1.0 W.

2.4 *In vitro* cell bioimaging

HeLa cells were incubated in Dulbecco's Modified Eagle's Medium supplemented with the hydrophilic $BaLaF_5$:Mn/Yb/Er UCNPs (200 μg/mL), 10% fetal bovine serum and 1% penicillin and streptomycin at 37 ℃ and 5% CO_2. After 4 h, the unbound UCNPs were washed several times with phosphate buffer solution (PBS). And the HeLa cells treated with these UCNPs were imaged by a commercial confocal laser scanning microscope (ZEISS LSM-710 NLO) equipped with a femtosecond-pulsed Ti: Sapphire laser and water immersion objective. The excitation beam with 980 nm wavelength was produced by the femtosecond laser with power of 600 mW. The green and red channels were recorded at the spectral regions of 500-600 and 600-700 nm, respectively.

2.5 Cytotoxicity assay

The *in vitro* viability of HeLa cells was measured via the 3-(4,5-dimethylthiazol-2-yl)-2,5-diphenyl-tetrazolium bromide (MTT) proliferation assay method. HeLa cells were seeded into a 96-well microplate (6000 cells per well) and then pre-incubated at 37 °C under 5% CO_2 for 3 h. Then, the cells were grown in Dulbecco's Modified Eagle's Medium (DMEM) solution containing different concentrations of $BaLaF_5$:20%Mn/20%Yb/2%Er UCNPs (100, 200, 400, and 600 $\mu g{\cdot}mL^{-1}$). These HeLa cells were incubated at 37 ℃ for another 20 h under 5% CO_2. Subsequently, each cell was added with 10 μL MTT labelling solution and then incubated further for 4 h at 37 ℃.

2.6 *In vivo* UC and X-ray imaging

To study the *in vivo* UC and X-ray dual-modal imaging, 10 wt% chloral hydrate solutions were intraperitoneally injected into the nude mouse firstly, then a certain amount (200 μL) of the hydrophilic $BaLaF_5$:Mn/Yb/Er UCNPs aqueous solution with concentration of 3 $mg{\cdot}mL^{-1}$ was subcutaneously injected. Finally, the UC/X-ray dual-modal imaging was carried out by a multi-modal *in vivo* imaging system (Bruker *In Vivo* FX PRO) with an external 980 nm laser as the excitation source and X-ray imaging functionality. The X-ray images were recorded under the operating voltage of 45 kVp. All animal procedures comply with the institutional animal use, approved by the Laboratory Animal Center of Hunan.

2.7 *Ex vivo* UC imaging

To reveal the distribution and accumulation of these hydrophilic $BaLaF_5$:Mn/Yb/Er UCNPs in various organs, 200 μL of these UCNPs with concentration of 3 $mg{\cdot}mL^{-1}$ was intravenously injected into the nude mouse at tail vein. After 0.5 h injection, the mouse was sacrificed and major organs including heart, lung, liver, spleen, and kidney were used to detect the UC signal by the *in vivo* imaging system (Bruker *In Vivo* FX PRO) with the similar conditions of the aforementioned UC imaging.

3. Results and discussions

3.1 Structure control

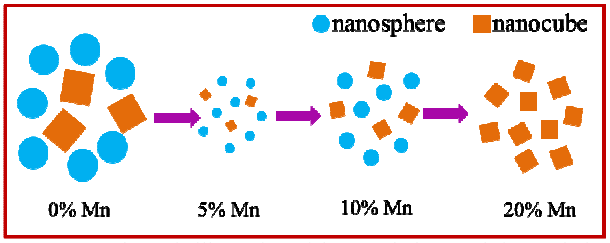

Scheme. 1 Schematic illustration of the morphology and size evolution of the UCNPs doped with different Mn^{2+} contents.

Scheme. 1 shows the schematic diagram of doping induced morphology and size control of $BaLaF_5$ UCNPs from large sphere to small cube, which is further demonstrated by later TEM and XRD results. Fig. 1 displays the XRD patterns of the as-prepared $BaLaF_5$ samples doped with different Mn^{2+} contents. As shown in Fig. 1, all the diffraction peaks of the as-prepared samples were matched well with the standard cubic phase of $BaLaF_5$ (JCPDS 48-0099). No extra impurity diffraction peaks were observed, indicating the formation of pure cubic phase structure. Notably, with increasing the Mn^{2+} content, the phase of the samples is still maintained, indicating the different Mn^{2+} content has no influence on the crystal phase in Ba-based host, which is different with our previous report for Mn^{2+} doped $NaLnF_4$ host.[59] In addition, compared with the Mn-free sample, the diffraction peaks of $BaLaF_5$ samples doped Mn^{2+} were broadened, indicating the decreased particle size. Moreover, the diffraction peaks gradually narrow with increasing Mn^{2+} content from 5% to 20%, suggesting an increasing in particle size, which is further verified by later TEM observation and size distribution. In addition, we have performed the Rietveld refinement on the experimental data using Jade 6.5 software. And the lattice constants of the $BaLaF_5$ doped with 0%, 5%, and 10% Mn^{2+} were calculated to 5.9853, 5.9797, and 5.9775 Å, respectively, indicating the Mn^{2+} was successfully incorporated into the host.

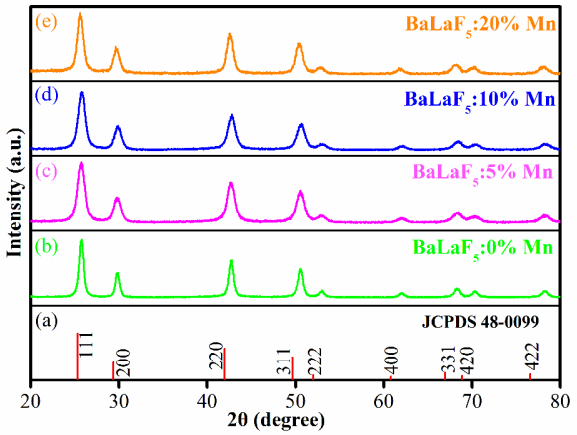

Fig. 1 XRD patterns of $BaLaF_5$:Yb/Er UCNPs doped with different Mn^{2+} contents: (b) 0%, (c) 5%, (d) 10% and (e) 20%. (a) the standard cubic phase structure (JCPDS-48-0099).

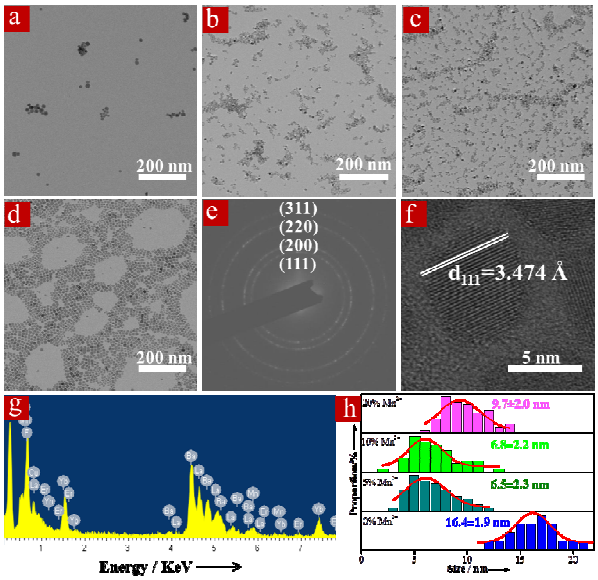

Fig. 2 TEM images of $BaLaF_5$ UCNPs doped with different Mn^{2+} contents: (a) 0%, (b) 5%, (c) 10% and (d) 20%; (e) the corresponding SAED image of 20% Mn doped sample; (f) HRTEM image of $BaLaF_5$ UCNPs doped with 20% Mn; (g) EDS result of $BaLaF_5$ UCNPs doped with 20% Mn; (h) the particle size distribution of $BaLaF_5$ UCNPs doped with different Mn^{2+} contents.

To further reveal the morphology and size evolution, the as-prepared Mn^{2+} doped $BaLaF_5$ UCNPs were characterized by TEM. Figs. 2a-d show the typical TEM images of the $BaLaF_5$ UCNPs doped with different Mn^{2+} contents. As demonstrated, all of the UCNPs possess high quality and monodispersed nature. With increasing Mn^{2+} contents from 5% to 20%, the morphology of the particles changed from sphere to cube (Figs. 2b-d). The selected area electron diffraction (SAED) pattern of 20% Mn^{2+} doped sample (Fig. 2e) reveal the formation of face-centered cubic structure, which is consistent with the aforementioned XRD analysis. The average sizes (Fig. 2h) of 0%, 5%, 10% and 20% Mn^{2+} doped $BaLaF_5$ UCNPs are measured to 16.4±1.9 nm, 6.5±2.3 nm, 6.8±2.2 nm, 9.7±2.0 nm, respectively, demonstrating the formation of sub-10 nm nanocrystals. The typical high-resolution TEM (HRTEM) image of an individual particle of $BaLaF_5$ doped with 20% Mn^{2+} sample shown in Fig. 2f reveals clear lattice fringes of the cubic phase (111) crystal plane with d-spacing of 3.474 Å. The element composition analyzed by energy-dispersive X-ray spectrometer (EDS) reveals the presence of Ba, La, F and doped Yb, Er, Mn, further verifying Mn^{2+} is successfully doped into the host matrix. Therefore, sub-10 nm ultra-small $BaLnF_5$ UCNPs with controlled shape and size can be achieved by only adjusting the doped Mn^{2+} contents, which provide a new route for synthesis of sub-10 nm Ba-based nanocrystals.

3.2 UC luminescent properties

The room-temperature UC luminescent spectra of $BaLaF_5$:20%Yb^{3+}/2%Er^{3+}/xMn^{2+} (x =0%, 5%, 10% and 20%) UCNPs were measured by a spectrophotometer under the excitation of 980 nm laser diode. As shown in Fig. 3a, all samples display green and red emission bands centered at 524/544 and 667 nm, respectively. The Mn-free sample possesses the most intense UC luminescence, which is attributed to the largest size of these particles. With increasing Mn^{2+} from 5% to 20%, the

intensity of UC luminescence increased due to the gradually increased particle size. When doping 20% Mn^{2+}, the UC luminescence intensity is similar to the Mn-free sample, while the size decreased to half, which demonstrated the UCNPs doped with 20% Mn^{2+} have great potential application in bioimaging. In addition, the red UC emission was not affected by doping Mn^{2+}, which is different with previous reports for Mn doping induced the enhancement of red UC emission.[59,60] Therefore, we speculate that the Mn^{2+} are mainly occupied the sites of Ba^{2+} owing to the same valence, not the Ln^{3+}, resulting in low energy transfer efficiency between Mn^{2+} and Er^{3+}. According to the energy level diagram (Fig. 3b), the red UC emission band centered at 667 nm is attributed to that the electron transfers from the $^4F_{9/2}$ level to the $^4I_{15/2}$ level of Er^{3+}. The green emission band of Er^{3+} centered at 524/544 nm are attributed to the electronic transition $^2H_{11/2}/^4S_{3/2} \rightarrow {}^4I_{15/2}$ of Er^{3+}. In addition, the corresponding CIE coordinates (Fig. S2) of the as-prepared samples doped with 5%, 10% and 20% Mn^{2+} are calculated to be (0.391, 0.595), (0.370, 0.616) and (0.342, 0.645), respectively.

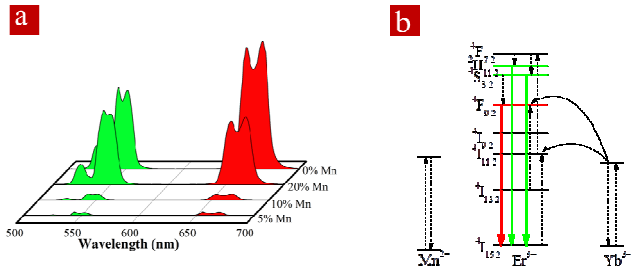

Fig. 3 (a) UC spectra of $BaLaF_5$ UCNPs doped with different Mn^{2+} contents, (b) the simplified energy diagram.

To further study the UC mechanism, the excitation power dependent green and red UC emissions was studied (Fig. S1a). In a general UC process, the UC luminescent intensity (I_{UC}) is proportional to the intensity of the near-infrared excitation light (I_{IR}), which can be described as the following formula: $I_{UC} \propto I_{IR}^{n}$. Where n is the number of photon absorbed for each UC emission. The value of n was determined by the slope of the fitted line in the plot of log I_{UC} versus log I_{IR}. Fig. S1b revealed that the slopes for the green and red UC emissions of Er^{3+} in Mn^{2+} doped $BaLaF_5$ UCNPs at 524, 544, and 667 nm are 1.61, 1.89 and 1.49, respectively, indicating that two photons were needed for the green and red emissions.

3.3 *In vitro* cell fluorescence bioimaging

Ultra-small sub-10 nm $BaLaF_5$: 20%Mn/20%Yb/2%Er UCNPs with intense UC luminescence were selected to further demonstrate the ability of application in *in vitro* cell imaging. Firstly, the hydrophobic $BaLaF_5$ sample was converted into hydrophilic with chloroform and SDS. Then, HeLa cells were incubated with the sub-10 nm $BaLaF_5$ UCNPs for 4 h at 37 ℃ and 5% CO_2, and finally the cells were imaged by confocal laser scanning microscopy (ZEISS LSM-710 NLO) under 980 nm excitation. As shown in Fig. 4b and c, intense green signal (500-600 nm) and red signal (600-700 nm) were observed on the surface of HeLa cells, indicating that these UCNPs were successfully internalized into the cells. The overlay image (Fig. 4d) shows the UC signals are matched well with HeLa cells. Moreover, as shown in the localized spectra taken from HeLa cells and background (inset of Fig. 4d), the characteristic green and red UC signals with absence of autofluorescence were observed, further demonstrating these UCNPs were grafted on the surface of HeLa cells. Based on the above analysis, these UCNPs can be used as ideal optical probes for bioimaging with no auto fluorescence.

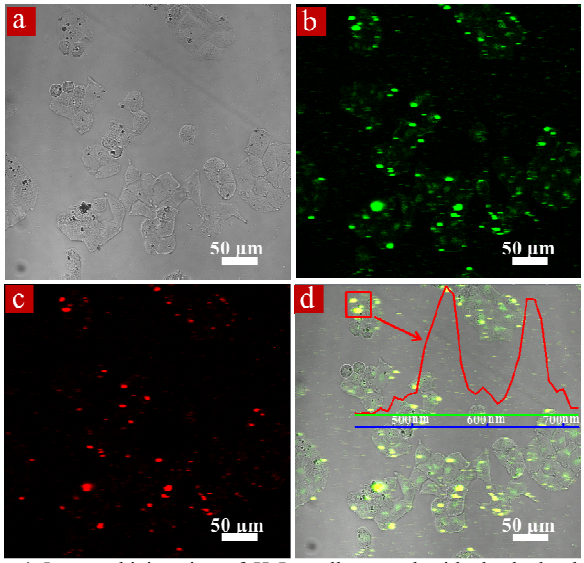

Fig. 4 *In vitro* bioimaging of HeLa cells treated with the hydrophilic $BaLaF_5$ UCNPs doped with 20% Mn^{2+} under 980 nm excitation: (a) bright field images, (b) and (c) the corresponding green (500-600 nm) and red (600-700 nm) luminescent images, respectively, (d) the overlay image. The inset of Fig. 4d shows the corresponding localized photoluminescence spectra taken from HeLa cells and background in the spectral range of 500 to 700 nm with a 980 nm excitation.

3.4 Cell cytotoxicity test

The cytotoxicity of the hydrophilic $BaLaF_5$ UCNPs in HeLa cells was measured by the MTT method. Fig. 5 shows the cell viability of the HeLa cells incubated with different concentrations of the SDS-modified $BaLaF_5$: 20%Mn/20%Yb/2%Er UCNPs at 37 ℃ and 5% CO_2 for 24 h. Compared with the cells untreated with the UCNPs, the viability of the HeLa cells decreased to 82% at the concentration of 100 $\mu g \cdot mL^{-1}$. No significant differences were observed when UCNPs concentration was increased to 400 $\mu g \cdot mL^{-1}$. The cellular viability was detected to 69% when the concentration of UCNPs was further increased to 600 $\mu g \cdot mL^{-1}$. These results demonstrate that the SDS-functionalized UCNPs (200 $\mu g \cdot mL^{-1}$) used in the above bioimaging have low cell toxicity. Therefore, the SDS-modified $BaLaF_5$ UCNPs with little cytotoxicity and excellent UC emission are promising candidates for optical bioimaging.

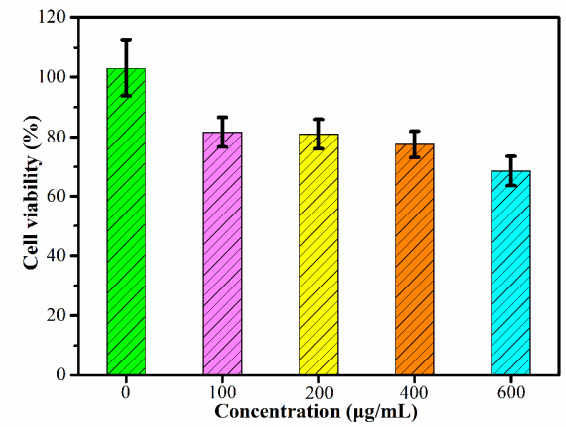

Fig. 5 Cell viability of HeLa cells treated with different concentrations of these SDS-modified $BaLaF_5$:20%Mn/20%Yb/2%Er UCNPs at 37 °C for 24 h under 5% CO_2.

3.5 *In vivo* UC luminescent imaging and synergistic UC/X-ray bioimaging

To further demonstrate the *in vivo* UC bioimaging, the hydrophilic $BaLaF_5$ UCNPs doped with 20% Mn^{2+} (200 μL, 3 $mg{\cdot}mL^{-1}$) was subcutaneously injected into a nude mouse. The UC images of the mouse were shown in Fig. S3, and a significant UC signal was observed after injection, while no signal was detected without injection of the sample. Fig. 6 shows the synergistic X-ray and UC bioimaging of the mouse subcutaneously injected with these hydrophilic UCNPs. The obvious X-ray absorption contrast (indicated by red arrow in Fig. 6b) and the high contrast UC signal (the middle panel of Fig. 6b) were observed at the same region, which shows the perfect overlap between the X-ray and UC signals. Therefore, these UCNPs can be used as synergistic dual-modal nanoprobes for combining the both advantages of the X-ray and UC bioimaging.

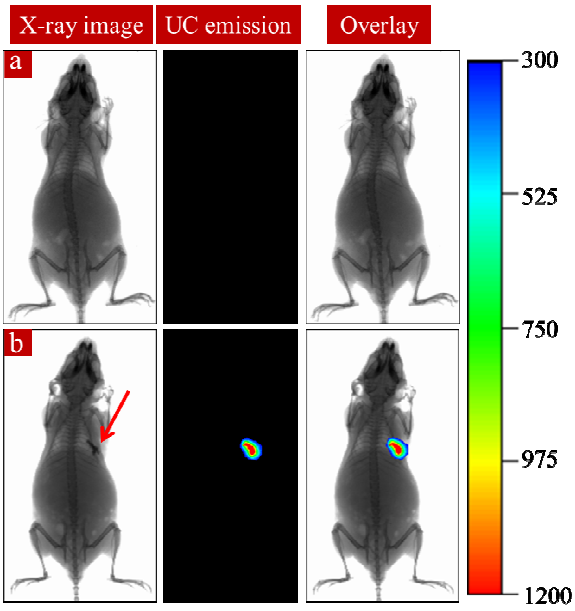

Fig. 6 *In vivo* X-ray and UC luminescent bioimaging of a nude mouse: (a) without subcutaneous injection of UCNPs, (b) with subcutaneous injection of UCNPs. The left panel: X-ray imaging, the middle panel: UC imaging, the right panel: the overlay images.

3.6 *Ex vivo* bioimaging

In order to investigate the distribution of these UCNPs in various organs, a mouse was intravenously injected with the hydrophilic UCNPs (200 μL, 3 $mg{\cdot}mL^{-1}$) via tail vein. After 0.5 h injection, the mouse was anatomized and major organs including heart, lung, liver, spleen and kidney were detected by *ex vivo* UC bioimaging. As shown in Fig. 7, the UC signals were clearly observed in the lung and no any signals were observed in the other organs of the mouse. The nanoparticles were mainly aggregated in the lung within 0.5 h post-injection, which was coincident with our reports about the distribution *in vivo* of $NaYbF_4$:Er UCNPs.[64] Meanwhile, Liu's report also revealed that the nanoparticles transferred from lung to liver with increasing time from 1 min to 24 h.[65] These results demonstrate that these UCNPs are mainly accumulated in lung at the initial time, which is beneficial for the detection of lung diseases.

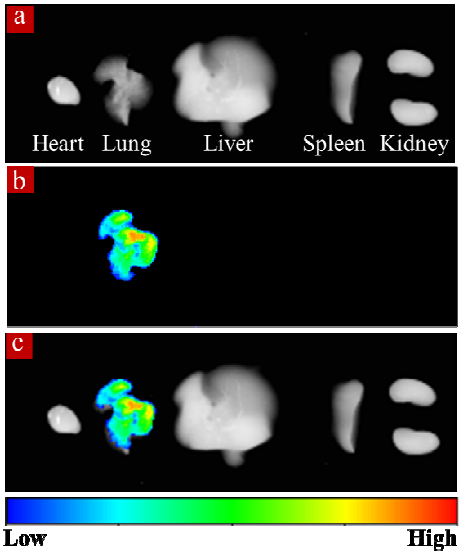

Fig. 7 *Ex vivo* UC luminescent imaging of the nude mouse after tail vein injection of the hydrophilic $BaLaF_5$ UCNPs doped with 20% Mn^{2+}: (a) bright field, (b) UC emission, (c) overlay.

Conclusions

In conclusion, sub-10 nm $BaLaF_5$:Mn/Yb/Er UCNPs for dual-modal X-ray and UC imaging was developed via a simplified solvothermal method. The XRD and TEM results reveal that the morphology and size of the as-prepared $BaLaF_5$ UCNPs can be tuned by controlling the Mn^{2+} content. The size of Mn^{2+} doped UCNPs decreased obviously compared with the Mn^{2+}-free sample and the morphology was tuned from sphere to cube with increasing Mn^{2+} content. The intense UC luminescent signal without auto-fluorescence was observed in HeLa cells treated with sub-10 nm $BaLaF_5$ nanocubes, and the little cytotoxicity further demonstrated these UCNPs are promising nanoprobes for *in vitro* cell imaging. Moreover, the well matched X-ray and UC signals in *in vivo* dual-modal bioimaging indicated these UCNPs have great potential for synergistic X-ray and UC imaging. Furthermore, the *ex vivo* UC imaging indicates these UCNPs are gathered at the lung at initial time, which demonstrated the samples can be used as ideal probe for detection of lung diseases.

Acknowledgments

This work was supported by the National Natural Science Foundation of China (Nos. 51102202, and 91230116), Specialized Research Fund for the Doctoral Program of Higher Education of China (No. 20114301120006) and Hunan Provincial Natural Science Foundation of China (Nos. 12JJ4056 and 13JJ1017), and Scientific Research Fund of Hunan Provincial Education Department (13B062). We thank Prof. Guoqiang Bi, Dr. Huijing Liu, and Dr. Xiaokang Zhang in University of Science and Technology of China for *in vitro* cell imaging and helpful discussions. We thank Prof. Jianhua Hao, Dr. Ming- Kiu Tsang, and Mr. Chi-Fai Chan, in The Hong Kong Polytechnic University for cell cytotoxicity assay.

Notes and references

[a] *College of Physics and Information Science and Key Laboratory of Low-dimensional Quantum Structures and Quantum Control of the Ministry of Education, Hunan Normal University, Changsha, Hunan, China. Email: songjunz@hunnu.edu.cn*

[b] *Faculty of Materials, Optoelectronics and Physics, Key Laboratory of Low-dimensional Materials and Application Technology (Ministry of Education), Xiangtan University, Xiangtan 411105, People's Republic of China.*

[c] *Department of Applied Physics and Materials Research Center, The Hong Kong Polytechnic University, Hong Kong.*

[d] *These authors contributed equally to this study.*

1 J. Zhou, Z. Liu and F. Y. Li, *Chem. Soc. Rev.*, 2012, **41**, 1323.
2 H. Y. Xing, S. J. Zhang, W. B. Bu, X. P. Zheng, L. J. Wang, Q. F. Xiao, D. L. Ni, J. M. Zhang, L. P. Zhou, W. J. Peng, K. L. Zhao, Y. Q. Hua and J. L. Shi, *Adv. Mater.*, 2014, DOI: 10.1002/adma.201305222.
3 N. M. Idris, M. K. Gnanasammandhan, J. Zhang, P. C. Ho, R. Mahendran and Y. Zhang, *Nature medcine*, 2012, **18**, 1580.
4 Y. L. Dai, H. H. Xiao, J. H. Liu, Q. H. Yuan, P. A. Ma, D. M. Yang, C. X. Li, Z. Y. Cheng, Z. Y. Hou, P. P. Yang and J. Lin, *J. Am. Chem. Soc.*, 2013, **135**, 18920.
5 J. H. Hao, Y. Zhang and X. H. Wei, *Angew. Chem. Int. Ed.*, 2011, **50**, 6876.
6 Y. S. Liu, D. T. Tu, H. M. Zhu and X. Y. Chen, *Chem. Soc. Rev.*, 2013, **42**, 6924.
7 Q. F. Xiao, X. P. Zhang, W. B. Bu, W. Q. Ge, S. J. Zhang, F. Chen, H. Y. Xing, Q. G. Ren, W. P. Fan, K. L. Zhao, Y. Q. Hua and J. L. Shi, *J. Am. Chem. Soc.*, 2013, **135**, 13041.
8 F. Wang, D. Banerjee, Y. S. Liu, X. Y. Chen and X. G. Liu, *Analyst*, 2010, **135**, 1839.
9 M. Wang, C. C. Mi, W. X. Wang, C. H. Liu, Y. F. Wu, Z. R. Xu, C. B. Mao and S. K. Xu, *ACS Nano*, 2009, **3**, 1580.
10 S. J. Zeng, H. B. Wang, W. Lu, Z. G. Yi, L. Rao, H. R. Liu and J. H. Hao, *Biomaterials*, 2014, **35**, 2934.
11 N. Bogdan, E. M. Rodríguez, F. Sanz-Rodríguez, M. C. I. de la Cruz, Á. Juarranz, D. Jaque, J. G. Solé and J. A. Capobianco, *Nanoscale*, 2012, **4**, 3647.
12 J. Shen, G. Y. Chen, T. Y. Ohulchanskyy, S. J. Kesseli, S. Buchholz, Z. P. Li, P. N. Prasad and G. Han, *small*, 2013, **9**, 3213.
13 F. C. J. M. van Veggel, C. H. Dong, N. J. J. Johnson and J. Pichaandi, *Nanoscale*, 2012, **4**, 7309.
14 M. Haase and H. Schäfer, *Angew. Chem. Int. Ed.*, 2011, **50**, 5808.
15 H. Dong, L. D. Sun and C. H. Yan, *Nanoscale*, 2013, **5**, 5703.
16 Y. F. Wang, G. Y. Liu, L. D. Sun, J. W. Xiao, J. C. Zhou and C. H. Yan, *ACS Nano*, 2013, **7**, 7200.
17 C. H. Dong, A. Korinek, B. Blasiak, B. Tomanek and F. C. J. M. van Veggel, *Chem. Mater.*, 2012, **24**, 1297.
18 G. F. Wang, Q. Peng and Y. D. Li, *Acc. Chem. Res.*, 2011, **44**, 322.
19 R. Heim, A. B. Cubitt and R. Y. Tsien, *Nature*, 1995, **373**, 663.
20 T. Jamieson, R. Bakhshi, D. Petrova, R. Pocock, M. Imani and A. M. Seifalian, *Biomaterials*, 2007, **28**, 4717.
21 X. H. Gao, Y. Y. Cui, R. M. Levenson, L. W. K. Chung and S. M. Nie, *Nat. Biotechnol*., 2004, **22**, 969.
22 G. Gao, C. L. Zhang, Z. J. Zhou, X. Zhang, J. B. Ma, C. Li, W. L. Jin and D. X. Cui, *Nanoscale*, 2013, **5**, 351.
23 Y. L. Liu, K. L. Ai, J. H. Liu, Q. H. Yuan, Y. Y. He and L. H. Lu, *Adv. Healthcare Mater.*, 2012, **1**, 461.
24 P. J. Dihingia and S. Rai, *J. Lumin.*, 2012, **132**, 1243.
25 C. X. Li, D. M. Yang, P. A. Ma, Y. Y. Chen, Y. Wu, Z. Y. Hou, Y. L. Dai, J. H. Zhao, C. P. Sui and J. Lin, *Small*, 2013, **9**, 4150.
26 F. Zhang, G. B. Braun, Y. F. Shi, Y. C. Zhang, X. H. Sun, N. O. Reich, D. Y. Zhao and G. D. Studky, *J. Am. Chem. Soc*., 2010, **132**, 2850.
27 X. Teng, Y. H. Zhu, W. Wei, S. C. Wang, J. F. Huang, R. Naccache, W. B. Hu, A. L. Y. Tok, Y. Han, Q. C. Zhang, Q. L. Fan, W. Huang, J. A. Capobianco and L. Huang, *J. Am. Chem. Soc.*, 2012, **134**, 8340.
28 F. Wang, Y. Han, C . S. Lim, Y. H. Lu, J. Wang, J. Xu, H. Y. Chen, C. Zhang, M. H. Hong and X. G. Liu, *Nature*, 2010, **463**, 1061.
29 H. Kobayashi, M. Ogawa, R. Alford, P. L. Choyke and Y. Urano, *Chem. Rev.*, 2010, **110**, 2620.
30 F. Zhang, Q. H. Shi, Y. C. Zhang, Y. F. Shi, K. L. Ding, D. Y. Zhao and G. D. Stucky, *Adv. Mater.*, 2011, **23**, 3775.
31 S. L. Gai, C. X. Li, P. P. Yang and J. Lin, *Chem. Rev.*, 2014, **114**, 2343.
32 C. Wang, L. Chen and Z. Liu, *Biomaterials*, 2011, **32**, 1110.
33 S. Jiang and Y. Zhang, *Langmuir*, 2010, **26**, 6689.
34 L. Cheng, K. Yang, Y. G. Li, J. H. Chen, C. Wang, M. W. Shao, S. T. Lee and Z. Liu, *Angew. Chem. Int. Ed.*, 2011, **50**, 7385.
35 M. Nyk, R. Kumar, T. Y. Ohulchanskyy, E. J. Bergey and P. N. Prasad, *Nano Lett.*, 2008, **8**, 3834.
36 Y. Sun, X. J. Zhu, J. J. Peng and F. Y. Li, *ACS Nano*, 2013, **7**, 11290.
37 X. J. Zhu, J. Zhou, M. Chen, M. Shi, W. Feng and F. Y. Li, *Biomaterials*, 2012, **33**, 4618.
38 J. Zhou, X. J. Zhu, M. Chen, Y. Sun and F. Y. Li, *Biomaterials*, 2012, **33**, 6201.
39 A. Xia, M. Chen, Y. Gao, D. M. Wu, W. Feng and F. Y. Li, *Biomaterials*, 2012, **33**, 5394.
40 Y. S. Liu, D. T. Tu, H. M. Zhu, E. Ma and X. Y. Chen, *Nanoscale*, 2013, **5**, 1369.
41 Q. Liu, Y. Sun, T. S. Yang, W. Feng, C. G. Li, F. Y. Li, *J. Am. Chem. Soc.*, 2011, **133**, 17122.
42 Y. Yang, Y. Sun, T. Y. Cao, J. J. Peng, Y. Liu, Y. Q. Wu, W. Feng, Y. J. Zhang and F. Y. Li, *Biomaterials*, 2013, **34**, 774.
43 F. Wang and X. G. Liu, *Chem. Soc. Rev.*, 2009, **38**, 976.
44 J. N. Liu, W. B. Bu, L. M. Pan and J. L. Shi, *Angew. Chem. Int. Ed.*, 2013, **52**, 4375.
45 C. Z. Zhao, X. G. Kong, X. M. Liu, L. P. Tu, F. Wu, Y. L. Zhang, K. Liu, Q. H. Zeng and H. Zhang, *Nanoscale*, 2013, **5**, 8084.
46 T. Y. Cao, Y. Yang, Y. Sun, Y. Q. Wu, Y. Gao, W. Feng and F. Y. Li, Biomaterials, 2013, **34**, 7127.
47 Q. W. Tian, J. Q. Hu, Y. H. Zhu, R. J. Zou, Z. G. Chen, S. P. Yang, R. W. Li, Q. Q. Su, Y. Han and X. G. Liu, *J. Am. Chem. Soc.*, 2013, **135**, 8571.
48 S. Sarkar, B. Meesaragandla, C. Hazra and V. Mahalingam, *Adv. Mater.*, 2013, **25**, 856.
49 K. W. K Krämer, D. Biner, G. Frei, H. U. Güdel, M. P. Hehlen and S. R. Lüthi, *Chem. Mater.*, 2004, **16**, 1244.
50 S. Sarkar, C. Hazra and V. Mahalingam, *Dalton. Trans.*, 2013, **42**, 63.
51 S. J. Zeng, M. K. Tsang, C. F. Chan, K. L. Wong, B. Fei and J. H. Hao, *Nanoscale*, 2012, **4**, 5118.
52 D. M. Yang, X. J. Kang, M. M. Shang, G. G. Li, C. Peng, C. X. Li and J. Lin, *Nanoscale*, 2011, **3**, 2589.
53 H. R. Liu, W. Lu, H. B. Wang, L. Rao, Z. G. Yi, S. J. Zeng and J. H. Hao, *Nanoscale*, 2013, **5**, 6023.
54 S. J. Zeng, M. K. Tsang, C. F. Chan, K. L. Wong and J. H. Hao, *Biomaterials*, 2012, **33**, 9232.

55 C. M. Zhang, P. A. Ma, C. X. Li, G. G. Li, S. S. Huang, D. M. Yang, M. M. Shang, X. J. Kang and J. Lin, *J. Mater. Chem.*, 2011, **21**, 717.

56 L. N. Guo, Y. Z. Wang, Y. H. Wang, J. Zhang and P. Y. Dong, *CrystEngComm*, 2012, **14**, 3131.

57 D. M. Yang, C. X. Li, G. Q. Li, M. M. Shang, X. J. Kang and J. Lin, *J. Mater. Chem.*, 2011, **21**, 5923.

58 F. Vetrone, V. Mahalingam and J. A. Capobianco, *Chem. Mater.*, 2009, **21**, 1847.

59 S. J. Zeng, Z. G. Yi, W. Lu, C. Qian, H. B. Wang, L. Rao, T. M. Zeng, H. R. Liu, H. J. Liu, B. Fei and J. H. Hao, *Adv. Funct. Mater.*, 2014, DOI: 10.1002/adfm. 201304270.

60 G. Tian, Z. J. Gu, L. J. Zhou, W. Y. Yin, X. X. Liu, L. Yan, S. Jin, W. L. Ren, G. M. Xing, S. J. Li and Y. L. Zhao, *Adv. Mater.*, 2012, **24**, 1226.

61 G. Z. Ren, S. J. Zeng and J. H. Hao, *J. Phys. Chem. C*, 2011, **115**, 20141.

62 X. Wang, J. Zhuang, Q. Peng and Y. D. Li, *Nature*, 2005, **437**, 121.

63 S. J. Zeng, J. J. Xiao, Q. B. Yang and J. H. Hao, *J. Mater. Chem.*, 2012, **22**, 9870.

64 Z. G. Yi, S. J. Zeng, W. Lu, H. B. Wang, L. Rao, H. R. Liu and J. H. Hao, *ACS Appl. Mater. Interfaces*, 2014, **6**, 3839.

65 C. Wang, L. Cheng, H. Xu and Z. Liu, *Biomaterials*, 2012, **33**, 4872.